Band structure and optical properties of $In_yGa_{1-y}As_{1-x}N_x$ alloys

C. Skierbiszewski, P. Perlin, P. Wisniewski, and T. Suski
UNIPRESS, High Pressure Research Center, Polish Academy of Sciences, Sokolowska 29, 01-142 Warsaw, Poland

J. F. Geisz
National Renewable Energy Laboratory, Golden, Colorado 80401

K. Hingerl
Profactor GmbH, Wehrgrabengasse 5, A-4400 Steyr, Austria

W. Jantsch
Institut fr Halbleiter- und Festkoerperphysik, Johannes-Kepler-Universitaet, A-4040 Linz, Austria

D. E. Mars
Agilent Laboratories, Palo Alto, California 94304

W. Walukiewicz
Materials Sciences Division, Lawrence Berkeley National Laboratory, Berkeley, California 94720
(Received 21 June 2001; published 19 December 2001)

We have carried out comprehensive studies of the nitrogen-induced modifications of the electronic structure of $In_yGa_{1-y}As_{1-x}N_x$ alloys. Temperature- and composition-dependent optical absorption spectra have been measured on free-standing layers of $In_yGa_{1-y}As_{1-x}N_x$ thin films lattice matched to GaAs with $0 \leqslant x = 3y \leqslant 0.025$ in the photon energy range 0.8–2.5 eV. The measurements provided information on the optical transitions at the Γ point of the Brillouin zone. Spectroscopic ellipsometry measurements performed in a wide photon energy range 1.5–5.5 eV have been used to determine the energy dependence of the dielectric function as well as energies of E_1, E_0', and E_2 critical point transitions. Measurements of the plasma edge frequency for samples with different electron concentrations have been used to determine the dispersion relation for the lowest conduction band. The results show a large effect of nitrogen on the optical spectra and on the dispersion relations for the conduction band states close to the Γ point. They can be consistently explained in terms of the recently proposed band anticrossing model. On the other hand, the observed small effect of N on the transition energies at the high-energy critical points can be well understood within a virtual crystal approximation. The insensitivity of the high-energy critical point transitions to the N content is in disagreement with the theoretical calculations predicting a large effect of N incorporation on the energies of *X* and *L* conduction band minima.

DOI: 10.1103/PhysRevB.65.035207 PACS number(s): 71.20.Nr, 78.20.Ci

I. INTRODUCTION

It has been shown recently that incorporation of small amounts of nitrogen into standard group III-V compounds leads to a large band gap reduction in the resulting $IIIN_xV_{1-x}$ alloys. Band gap reductions as large as 0.18 eV have been observed in $GaAs_{1-x}N_x$ with only 1% of N.[1–4] Similar effects were also observed in GaNP,[5,6] InNP,[7,8] GaNSbAs,[9] and InNSb (Ref. 10) alloys. Since addition of In or Sb to GaN_xAs_{1-x} compensates the N-induced contraction of the lattice parameter and further reduces the band gap, it is possible to grow $In_yGa_{1-y}N_xAs_{1-x}$ or $GaN_xSb_yAs_{1-x-y}$ quaternaries that are lattice matched to GaAs or InP and have energy gaps in the 1.3 to 1.55 μm spectral range. For example, $In_yGa_{1-y}N_xAs_{1-x}$ with $y=3x$ is lattice matched to GaAs. These discoveries generated considerable interest and opened an interesting possibility of using group $IIIN_xV_{1-x}$ alloys for a variety of optoelectronic applications.[11–13] So far, most of the investigations of InGaAsN alloys have been focused on the optical transitions at the energies close to the fundamental band gap. Measurements of the higher-energy E_1 and $E_1+\Delta_1$ transitions at critical points along the *L* direction of the Brillouin zone have shown that alloying of GaAs with GaN leads to a line broadening but has a very small effect on the transition energy.[14–18] Over the last several years a significant effort has been made to understand the physical origin of the unusually large effects of N on the electronic structure of $IIIN_xV_{1-x}$ alloys. To explain the large band reduction in GaNAs, Sakai *et al.*[19] have used the phenomenological dielectric model originally proposed by Van Vechten and Bergstresser.[20] The model predicts very large band gap bowing in all $IIIN_xV_{1-x}$ alloys and was later used by many workers to interpret the band gap reductions in a variety of semiconductor alloy systems. However, it has been found that at higher N compositions the band gap reductions predicted by the dielectric model were much larger than those observed experimentally. The early attempts to use first-principles, supercell calculations encountered a difficult problem as these methods could only consider ordered alloys.[2,21,22] Also, because of the limited size of the supercell, the calculations were limited to a few discrete compositions with rather large N content and could not be verified experi-

mentally. Still based on such first-principles supercell calculations Wei and Zunger[2] were able to explain the large, N-induced gap reduction in $GaAs_{1-x}N_x$ alloys in terms of a composition-dependent bowing parameter. They argued that the bowing parameter could be decomposed into three different contributions: volume deformation, charge exchange, and structural relaxation. Random alloys were theoretically treated by Bellaiche *et al.*[23] using the empirical psuedopotential method. The authors found that for $GaAs_{1-x}N_x$ with $x \leqslant 0.05$ about 20% of the total band gap reduction originates from the upward shift of the valence band edge. New challenges for band structure theories have been posed by a series of recent high-hydrostatic-pressure experiments. A greatly reduced and strongly nonlinear pressure dependence of the fundamental band gap has been measured in InGaAsN alloys.[24–26] Also, an additional N-related optical transition E_+ was discovered in these alloys.[25,27] To explain these new experiments a theoretical model has been proposed that describes the electronic structures of InGaAsN alloys in terms of an anticrossing interaction between the localized A_1 symmetry state of nitrogen and the extended conduction band states of the semiconductor matrix.[25,28,29] The significant, practical advantage of the band anticrossing (BAC) model is that it provides simple analytic expressions for the conduction band dispersion. The formula for the lower E_- and upper E_+ conduction subband is given by

$$E_{\pm}(k)=\frac{1}{2}[(E_M(k)+E_N)\pm\sqrt{(E_M(k)-E_N)^2+4xC_{MN}^2}], \tag{1}$$

where $E_M(k)$ is the energy of the conduction band of the semiconductor matrix, E_N is the energy position of the nitrogen-related level with A_1 symmetry, x is the nitrogen molar fraction, and C_{MN} is the hybridization matrix element. Later O'Reilly and Lindsay have proposed a modified version of the band anticrossing model that includes an interaction of the conduction and valence bands within the $\mathbf{k}\cdot\mathbf{p}$ approximation.[30] It should be noted that the dispersion relations given by Eq. (1) are analogous to those obtained within a coherent potential approximation (CPA) for a system of randomly distributed impurities interacting with a delocalized band.[31] Based on the dispersion relations given by Eq. (1) and shown in Fig. 1 a number of new effects including an enhancement of the electron effective mass[32] and improved donor activation efficiency in InGaNAs alloys[33] have been predicted and experimentally confirmed. Also the BAC model accounted very well for the pressure dependence of the interband transitions in GaNP (Ref. 34) and A_1 composition dependence of the E_+ and E_- transitions in AlGaNAs alloys.[16] It has been shown, most recently, that the BAC model also applies to ZnS_xTe_{1-x} and $ZnSe_yTe_{1-y}$, a new class of highly mismatched group II-VI semiconductor alloys that exhibit large band gap bowing parameters and strongly nonlinear pressure dependence of the band gap.[35] In response to the new experimental developments alternative interpretations of the composition and/or pressure dependence of the band gap of InGaNAs have been put forward by several research groups.[26,36–38] It has been argued that incorporation of

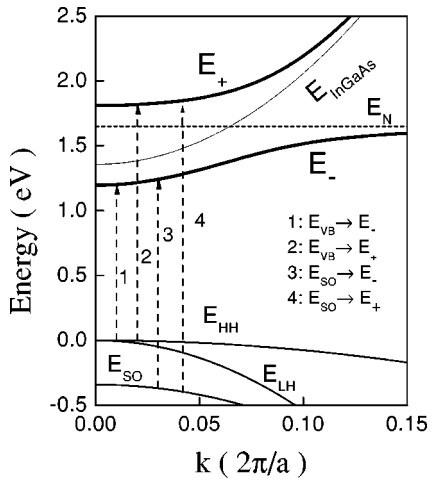

FIG. 1. Conduction band splitting and dispersion in $Ga_{0.96}In_{0.04}As_{0.99}N_{0.01}$ according to the band anticrossing model from Refs. 25 and 28. Arrows indicate different optical transitions.

nitrogen into GaAs breaks the symmetry leading to a splitting of the degenerate X and L minima and an interaction between electronic states of X, L, and Γ minima. The calculations of the conduction band structure based on the local density approximations (LDA's) performed by several groups gave quantitatively different results and faced the difficult problem of a unique identification of the origin of E_+ transitions. Calculations of Jones *et al.*[26] question the existence of such transitions whereas Mattila *et al.*[36] attribute the E_+ edge to a convolution of optical transitions to three widely energetically spread levels in the conduction band. The most recent calculations[39] have identified and calculated the pressure dependence of the levels responsible for the E_+ transitions in $GaN_{0.03}As_{0.97}$. Unfortunately, these calculations cannot be compared with experiment as the existing experimental results on the pressure dependence of the interband optical transitions are limited to samples with lower N content.[25] An entirely different interpretation of the effect of N on the band gap of InGaAsN alloys has been recently proposed by Al-Yacoub and Bellaiche.[40] Using a supercell pseudopotential technique the authors find that in the case of random InGaAsN alloys the dominant contribution to the downward shift of the conduction band (CB) edge originates from the first-order term in the perturbation of the Γ minimum states by the potential of the substitutional N. The role of the coupling between Γ, X, and L states which played a primary role in the LDA-based theories is found to be only of secondary importance in these new calculations. Finally, Zhang *et al.*[41] have proposed that the band gap reduction in GaNAs alloys can be explained by a broadening and downward shift of interacting N-related levels in a manner similar to the commonly observed band gap narrowing in heavily doped semiconductors. In order to test some of the predictions of these different theoretical models we have carried out a comprehensive study of the electronic structure of InGaNAs alloys. One of the major differences between the BAC model and the LDA-based calculations is the extent to which the higher-energy conduction band minima are affected by the substitutional N atoms. We use optical absorp-

tion and ellipsometry to determine the interband optical transitions in a wide photon energy range 0.8–5.5 eV. The energy-dependent electron effective mass is derived from measurement of the plasma frequency in *n*-type samples with the electron concentration ranging from 1×10^{17} cm^{-3} to 2×10^{19} cm^{-3}. The experimental results are compared with the predictions of the different theoretical models.

II. SAMPLE PREPARATION

The $In_yGa_{1-y}As_{1-x}N_x$ samples used in this study were grown by either metal-organic-vapor-deposition (MOCVD) or molecular beam epitaxy (MBE). The thin films were closely lattice matched to GaAs substrates by maintaining the In to N composition ratio $y=3x$. Details of the crystal growth are given elsewhere.[13,24] In order to measure the absorption coefficient in a wide photon energy range we have grown a specially designed structure that allowed separation of the layer from the substrate. The InGaAsN samples grown on a semi-insulating GaAs substrate consists typically of a 0.1-μm-thick GaAs buffer followed by a 100-nm-thick GaAsP (or AlGaAs) etch stop layer and then by a 1–2-μm-thick $In_yGa_{1-y}As_{1-x}N_x$ layer. The etching procedure used to remove the substrate and to secure the thin InGaAsN layers by sapphire or glass is described in Refs. 42 and 43. Both the glass and sapphire substrates are well transparent in the spectral range of 0.8–2.5 eV, where the transmission experiments were performed. The spectroscopic ellipsometry measurements were carried out on the same layers, but without removing the substrates. The electron effective mass was determined from infrared reflectivity experiments on 1–3-μm-thick MOCVD-grown $In_yGa_{1-y}As_{1-x}N_x$ layers deposited on semi-insulating GaAs. The layers were doped with Se and had electron concentrations ranging from 1×10^{17} cm^{-3} to 2×10^{19} cm^{-3}. The layer thickness for all samples was determined by scanning electron microscopy. The electron concentration was determined from Hall effect measurements.

III. INTERBAND ABSORPTION OF FREE-STANDING EPITAXIAL LAYERS

We have measured the interband optical absorption of five free-standing samples of $In_yGa_{1-y}As_{1-x}N_x$ with $0\leqslant x\leqslant0.025$ and $0\leqslant y\leqslant0.09$ in the photon energy range 0.8–2.2 eV. The absorption coefficients measured on free-standing GaAs and $In_{0.04}Ga_{0.96}As_{0.99}N_{0.01}$ layers are compared in Fig. 2. We find that the fundamental absorption edge shifts towards lower energies: the arrows in Fig. 2 indicate the band gap of GaAs, E_g, and of InGaNAs, E_-. The higher energy transition from the spin-orbit split-off valence band to the CB, denoted as $E_g+\Delta_{so}$ and $E_-+\Delta_{so}$, are also shown in Fig. 2. An additional absorption edge, denoted by E_+, is clearly observed. The onset of the absorption edge for $E_-+\Delta_{so}$ and E_+ was determined by the intersection of the extrapolated linear part of the absorption coefficient spectrum with the base line of the absorption indicated by the dashed lines in Fig. 2. We attribute the additional structure in the absorption edge of InGaAsN to a splitting of the conduction band. New absorption edges associated with optical

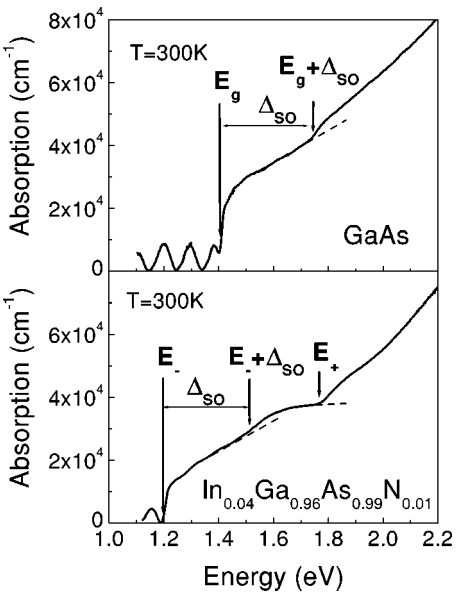

FIG. 2. Absorption of free-standing GaAs and InGaAsN layers. Positions of the energy gap E_g, $E_g+\Delta_{so}$ for GaAs and E_-, $E_-+\Delta_{so}$, E_+ for InGaAs are indicated by the arrows.

transitions from the spin-orbit split-off band to the lower conduction subband at 1.55 eV and from the top of the valence band to the upper subband at 1.85 eV are identified as $E_-+\Delta_{so}$ and E_+, respectively. All those transitions are schematically depicted in Fig. 1 within the framework of the BAC model. We will discuss in the next paragraph in detail the N alloy dependences of these transitions—together with higher-energy optical transitions. As is seen in Fig. 2 we observed a significant reduction of the absorption coefficient $\alpha(E)$ at the absorption edge of InGaAsN related to E_- in comparison to GaAs. The absorption coefficient of about 2.4×10^4 cm^{-1} is reduced to 1.1×10^4 cm^{-1} in $In_{0.04}Ga_{0.96}As_{0.99}N_{0.01}$. This reduction of the value of α can be understood within the framework of the BAC model. The anticrossing interaction admixes localized N-like wave function to the lowest conduction band edge states. The localized state component is only very weakly optically coupled to the valence band states, resulting in a reduced absorption coefficient. We have calculated $\alpha(E)$ for InGaAsN layer using the approach described earlier,[42] where our preliminary results obtained at room-temperature (RT) absorption were discussed. Since the simple BAC model does not account for temperature broadening effects, we compare now its predictions with data taken at low temperature where such effects can be neglected. The dots in Fig. 3 represent the experimentally determined $\alpha(E)$ measured at $T=10$ K in an MBE-grown $In_{0.04}Ga_{0.96}As_{0.99}N_{0.01}$ layer. The solid line represents calculations based on the BAC model with $E_N=1.65$ eV and $C_{MN}=2.7$ eV. The model quite well describes the spectral dependence of the absorption coefficient in the wide photon energy range. The discrepancies between the experimental data and theoretical calculations evident for the photon energies close to the $E_{VB}\rightarrow E_+$ transitions underscore the need for a more accurate description of the optical coupling matrix element for the higher-energy transitions. More detail

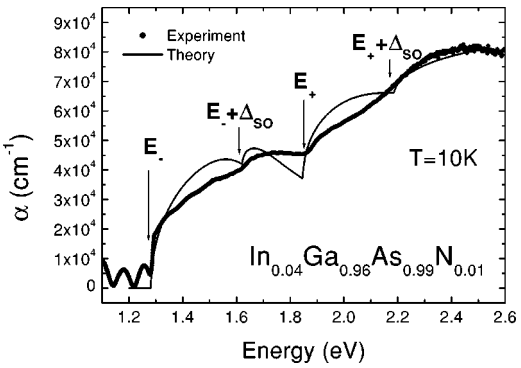

FIG. 3. Absorption spectrum of $Ga_{0.96}In_{0.04}As_{0.99}N_{0.01}$ layer at $T=10$ K (points) and calculation based on the band anticrossing model (according to Ref. 42). Points show the experimental data. The calculated curves show contributions from the transitions between three valence bands and two conduction subbands.

measurements of the temperature dependence of the absorption coefficient close to the E_- and E_+ absorption edges were performed on free-standing MBE- and MOCVD-grown layers. To analyze the change of the interband absorption edges with temperature we have plotted, in Figs. 4(a) and 4(b), $\alpha^2(E)$ as functions of the photon energy at the energies close to the E_- and E_+ transitions. As can be seen in Fig. 4(b), the squared absorption coefficients $\alpha^2(E)$ show a linear dependence on the photon energy, indicating that direct optical transitions are responsible for the E_+ absorption edge. The extrapolation of the linear part of $\alpha^2(E)$ to zero for the E_- transitions in Fig. 4(a) or to a constant offset value for E_+ transitions in Fig. 4(b) allows a determination of the

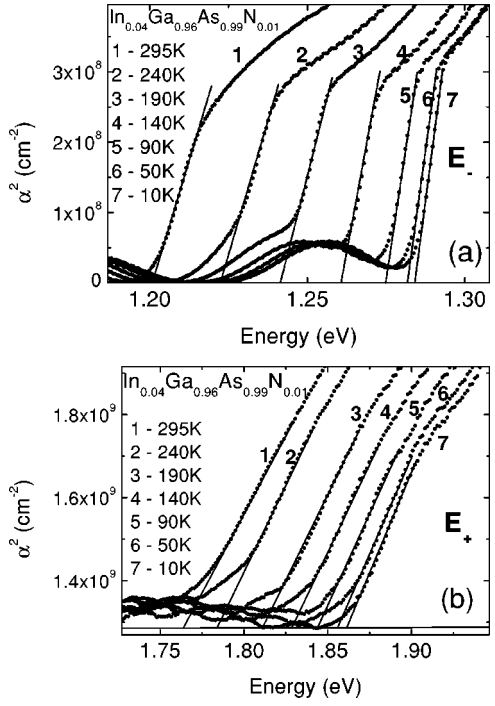

FIG. 4. Temperature dependence of the square of the absorption coefficient, $\alpha^2(E)$, for the E_- (a) and the E_+ (b) transitions, respectively.

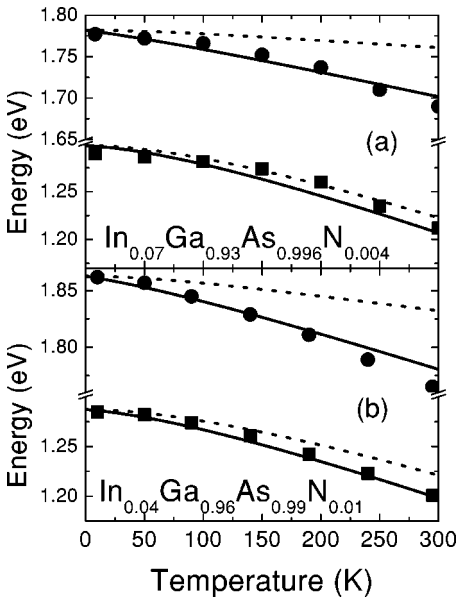

FIG. 5. Optical transitions E_- (squares) and E_+ (dots) obtained from absorption experiments on free-standing MBE (a) and MOCVD (b) layers. Dashed lines: calculations according to the BAC model with E_N constant. Solid lines: BAC model with E_N temperature-dependent $dE_N/dT=-0.25$ meV/K.

onset energies of the absorption edges for these two types of transitions. Temperature dependences of the E_- and E_+ energy edges for MBE and MOCVD layers are given in Fig. 5. In agreement with previously reported results[44] we find that in InGaAsN alloys the E_- energy exhibits a weaker temperature dependence than that observed in the N-free InGaAs matrix. Surprisingly the E_+ shows a somewhat stronger temperature dependence than E_-. The temperature dependence of the E_- and E_+ transitions can be useful for testing InGaAsN band structure models as was done before for other semiconductors.[45] In general, the temperature change of the energy gap in the linear approximation is defined by the following equation: $\Delta E_g(T)=D_g\alpha_T T-\beta_{e\text{-}ph}T$, where D_g is the energy gap deformation potential, α_T is the volume expansion coefficient, and $\beta_{e\text{-}ph}$ is the electron-phonon interaction.[24,45] D_g is a product of the pressure coefficient of the energy gap and bulk modulus. The pressure coefficients of E_- and E_+ for the $In_{0.04}Ga_{0.96}As_{0.99}N_{0.01}$ sample we have measured in transmission experiments in a diamond anvil cell: $dE_-/dp=80$ meV/GPa and $dE_+/dp=25$ meV/GPa, which is consistent with the data obtained in the photoreflectivity experiments in Ref. 25. This gives $D_g=-6$ eV for E_- and $D_g=-1.8$ eV for E_+. We use value of bulk modulus of GaAs, since In and N mole fractions are small. As was pointed out in Ref. 24 the reduction of the temperature dependence of the E_- in InGaAsN in comparison to GaAs can be associated solely with the reduction of the deformation potential (for GaAs, D_g is -7 eV). We find, however, that to explain the $E_+(T)$ dependence also a change of the electron-phonon interaction part is necessary. Keeping $\beta_{e\text{-}ph}$ constant for both transitions less pronounced changes of $E_+(T)$ than $E_-(T)$ are expected in the framework with this approach.

According to the BAC model the change in the position of

the E_+ transition should closely follow the temperature dependence of the N-related states. This means that the observed change of the E_+ energy with temperature reflects the temperature dependence of $A_1(N)$. We have calculated $E_-(T)$ and $E_+(T)$ using Eq. (1) of the BAC model and assuming linear dependence of the N-related A_1 state, $E_N(T)=1.68$ eV$+a_N T$. The temperature dependence of the InGaAs host matrix $E_M(T)$ can be determined using the well-known Varshni function $E_M(T)=E_g^{InGaAs}-\alpha(T^2/\beta+T)$ or the Bose-Einstein expression $E_M(T)=E_g^{InGaAs}-a/[e^{\theta/T}-1]$ where E_g^{InGaAs} is the band edge energy at $T=0$ K, a is the electron average phonon coupling constant, and θ is the average phonon temperature.[45] The temperature dependence of the InGaAs host matrix was assumed the same as for GaAs since the In mole fraction is small. In our fittings we used the Varshni function with GaAs parameters[46] $\alpha=5.408\times10^{-4}$ eV/K, $\beta=204$ K (both Varshni and Bose-Einstein relations describe well the temperature dependence of GaAs). The band edge of InGaAs at $T=0$ K was calculated with formula $E_g^{InGaAs}=1.512-1.337x+0.27x^2$ (eV) where x is the In content.[47] The dotted and solid lines in Figs. 5(a) and 5(b) were obtained for $a_N=0$ and $a_N=-0.25$ meV/K, respectively. A constant, temperature-independent value of the hybridization constant $C_{MN}=2.7$ eV was assumed in the calculation. These results appear to indicate a relatively strong temperature dependence of the N-level energy. They should be treated cautiously, however, since we have ignored the band edge broadening effects that are definitely more important in InGaAsN than in InGaAs ternaries. From absorption experiments we were also able to determine the temperature dependence of the spin-orbit splitting Δ_{so} which is almost constant in InGaAsN and equal to 0.34 eV.

IV. DIELECTRIC FUNCTION AND THE CRITICAL POINT TRANSITIONS

The results of the absorption measurements on the free-standing layers show a large effect of N incorporation on the optical transition close the lowest minimum of the conduction band. All the effects can be well explained by the BAC model. However, as has been mentioned in the Introduction some of the theories of the electronic structure of InGaAsN alloys claim that the presence of N in InGaAsN leads to a strong coupling of the electronic states at Γ, X, and L minima. To test the predictions of these theories we use spectroscopic ellipsometry (SE) to determine the energies of the optical transitions at E_1, $E_1+\Delta_1$, E_0', and E_2 in strain-free $In_yGa_{1-y}As_{1-x}N_x$ films ($y=3x$). The locations of the critical point (CP) transitions corresponding to different van Hove singularities in the case of GaAs are schematically shown in Fig. 6. The SE measurements were performed with an automatic and commercially available spectroscopic ellipsometer using a photoelastic modulator. The sampling distance was 10 meV in the photon energy range of 1.5–5.5 eV. All the spectra were taken at an angle of incidence, Θ, of 70.4°. We used the same samples as for transmission experiments but without the etching procedure. The dielectric function ϵ has been determined from the measured ellipsometric angles Ψ and Δ. The complex reflectance ratio r can be expressed in terms of the ellipsometric angles Ψ and Δ,

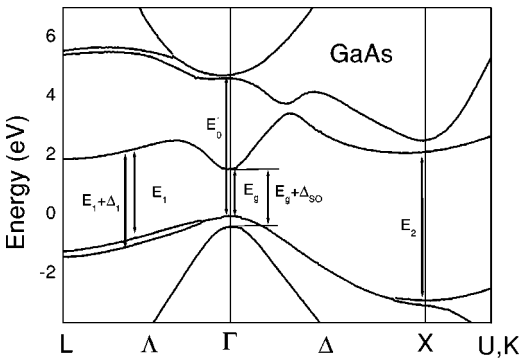

FIG. 6. Band structure of GaAs showing the main interband critical point transitions, after Ref 51.

$$\rho=\frac{r_p}{r_s}=\tan\Psi e^{i\Delta}, \tag{2}$$

where r_p and r_s are the reflection coefficients for light polarized parallel and perpendicular to the plane of incidence, respectively. This can be converted into the pseudodielectric function ϵ^* within the two-phase model (air/substrate):

$$\epsilon^*=\sin^2(\Theta)+\sin^2(\Theta)\tan^2(\Theta)\frac{(1-\rho)^2}{(1+\rho)^2}. \tag{3}$$

The details of the derivation of ϵ^* can be found in Ref. 48. The pseudodielectric function contains information about the dielectric function of (a) the GaAs substrate, (b) the InGaAsN layer, and (c) the oxide cap layer. The thickness of the oxide layers in our samples has been determined by comparing our results obtained on a GaAs reference layer with the literature data[48] where the oxide layer was removed from the sample. We have found that there was a 30-Å-thick oxide layer on our GaAs reference sample and we have assumed the same oxide thickness to be present on the InGaAsN films. The value of the bulk dielectric function ϵ has been then obtained by numerically removing the effects of the 30-Å-thick oxide layer from the data. The presence of the oxide layer mainly changes the intensity of the high-energy transitions around E_0' and E_2 CP's. Since the penetration depth of light at the CP photon energies is less than 500 Å and since the thickness of the InGaNAs films is larger than 1000 Å any effects of the sublayer part of the structure on ρ can be safely ignored. The real and imaginary parts of the bulk dielectric function ϵ of GaAs and of three InGaNAs samples are shown in Fig. 7. It is seen that with increasing N content, the E_1 and $E_1+\Delta_1$ structures around 2.9–3 eV are smeared out due to a disorder in the quaternary compounds as observed previously for CdHgTe (Ref. 49) and for AlGaInP (Ref. 50). The broadening is much less pronounced for the E_0' and E_2 CP's around 4.5 and 4.9 eV. In order to resolve the spectroscopic features close to the CP's, we have numerically calculated the second derivative of the experi-

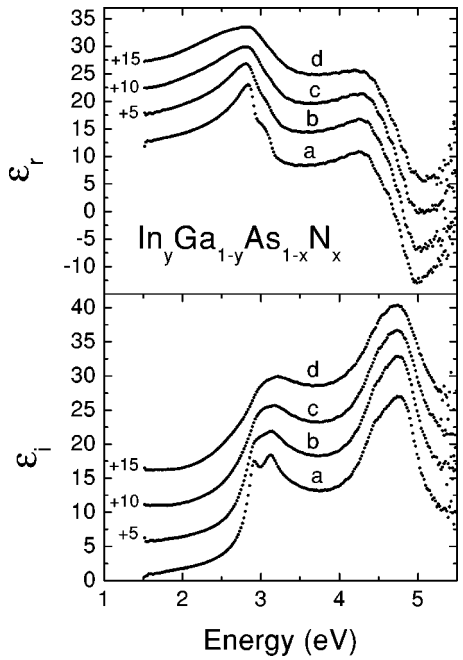

FIG. 7. Real (ϵ_r) and imaginary (ϵ_i) parts of the dielectric function in $In_yGa_{1-y}As_{1-x}N_x$ alloys after numerical removal of the influence from the oxide layer: *a*, GaAs; *b*, $x=0.004$, $y=0.07$; *c*, $x=0.0164$, $y=0.05$; *d*, $x=0.0247$, $y=0.08$. The curves *b*, *c*, and *d* are shifted by 5, 10, and 15, respectively.

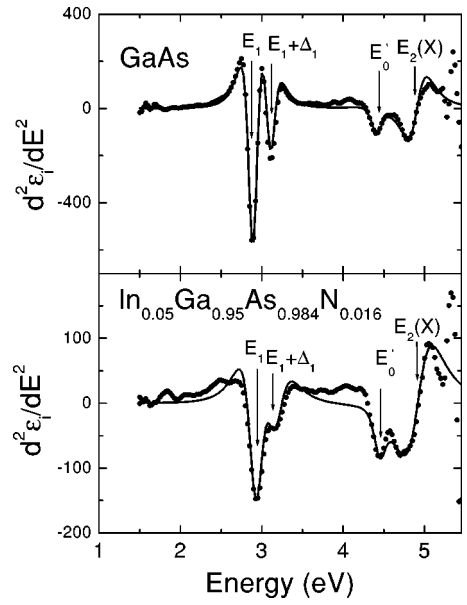

FIG. 8. Second derivative of the imaginary part of the dielectric function for GaAs and InGaAsN layers, respectively. The appropriate critical points transitions are indicated by arrows. Dots: experimental data. Solid lines: fits according to the critical point analysis.

mental complex dielectric function with respect to energy. The results are fitted with $\partial^2\epsilon/\partial E^2$ given by the expressions

$$\frac{\partial^2\epsilon}{\partial E^2}=-n(n-1)Ae^{i\phi}(E-E_{CP}+i\Gamma_{CP})^{n-2} \quad \text{for } n\neq 0 \tag{4a}$$

and

$$\frac{\partial^2\epsilon}{\partial E^2}=Ae^{i\phi}(E-E_{CP}+i\Gamma_{CP})^{-2} \quad \text{for } n=0. \tag{4b}$$

The only free parameters in the fitting procedure were Γ_{CP} and E_{CP}. The exponent n and the phase angle ϕ were chosen using arguments of Ref. 51. If the conduction and valence bands are strictly parallel, the E_1 and $E_1+\Delta_1$ transitions are two-dimensional (2D) CP's with $n=0$. The corresponding phase angle at RT is $\pi/2$. It should be emphasized, however, that, as has been shown in Ref. 51, fitting of the E_1 transition with an excitonic line shape ($n=-1$) results only in minor changes less than 10 meV in the resonance energies of the critical points. Therefore we adopted this procedure also for fitting spectra in the samples with the N content up to 2.5% and we determine E_{CP} at the E_1, $E_1+\Delta_1$, E_0', and E_2 transitions with the n and ϕ parameters of GaAs and InGaAsN. Figure 8 shows an example of the second derivative of the imaginary part of ϵ: The dots show our experimental results while the solid lines are the fitting curves. The arrows indicate the various transitions. In order to determine the transition energies more carefully we fitted both the real and imaginary parts of ϵ independently. All our experimental results on the interband optical transitions obtained from the optical absorption and SE measurements are combined in Fig. 9. The figure shows all optical transition at the energy range 0.8 eV up to 5.5 eV as functions of N content in InGaAsN. The error in determination of the transition energies is ± 10 meV for E_+ and E_- transitions: ± 25 meV for the E_1 and $E_1+\Delta_1$ transitions and about ± 40 meV for the E_0' and E_2 transitions. The results in Fig.

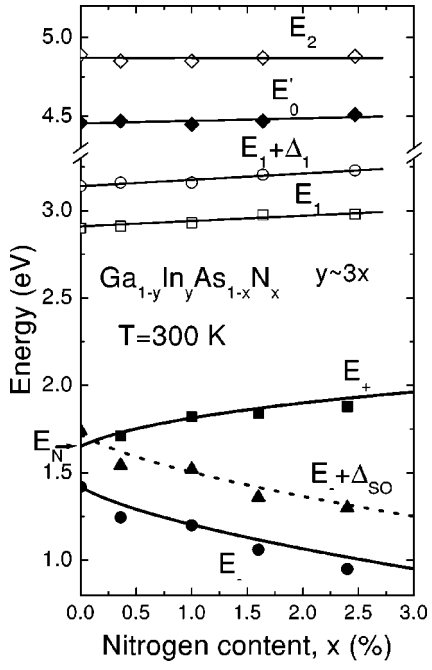

FIG. 9. Composition dependence of E_-, $E_-+\Delta_{so}$, and E_+ transitions measured in transmission and E_1, $E_1+\Delta_1$, E_0', E_2 obtained from spectroscopic ellipsometry.

9 show a dramatic difference in the N-composition dependence of the low-energy E_- and E_+ transitions at the Γ point compared with the higher-energy critical point transitions. The E_- and E_+ transitions show a very strong, nonlinear dependence on the N content. This dependence can be well explained by the BAC model. The solid lines show the calculated dependences for E_- and E_+ using Eq. (1) with $E_N=1.65$ eV and $C_{MN}=2.7$ eV.[25,28] The dashed line represents the behavior of the $E_-+\Delta_{so}$ transition calculated also within the BAC model assuming a constant N-independent spin-orbit splitting $\Delta_{so}=0.34$ eV. A good agreement with the experiment indicates that at these low compositions alloying of InGaAs with N has a negligible effect on the valence band structure. In strong contrast to the behavior of E_- and E_+ absorption edges, the higher-energy E_1, $E_1+\Delta_1$, E_0', and E_2 transitions show a very weak linear dependence on the N content. This behavior can be well understood within a virtual crystal approximation that accounts for the small gradual shift of the transition energy with the N content. The linear extrapolations of the energies of the E_1 and E_2 transitions agree reasonably well with the energies of about 6 eV predicted for both transitions in cubic GaN.[52] Also the energy positions of the valence bands seem to be unchanged—the values of the Δ_{so} and Δ_1 remain constant with the N content and are equal to the 0.34 eV and 0.25 eV respectively.

V. CONDUCTION BAND DISPERSION

One of the most striking features of the conduction band structure predicted by the BAC model is, as shown in Fig. 1, distinct flattening in the $E_-(k)$ dependence for the electron energies approaching E_N. To test this prediction we have measured the electron effective mass versus energy in $In_{0.03}Ga_{0.97}As_{0.99}N_{0.01}$ samples. The alloy composition of the samples was kept constant to avoid variations of the effective mass with the N content. The Fermi energy of electrons has been varied with doping. Samples doped with Se had the electron concentration in the range $1\times10^{17}-2\times10^{19}$ cm^{-3}. Infrared reflectivity has been used to measure the plasma edge frequency and the Hall effect has been used to determine the electron concentration. The effective mass of mobile electrons is defined as

$$\frac{1}{m_{\pm}^*(k)}=\frac{1}{\hbar^2 k}\left|\frac{dE_{\pm}(k)}{dk}\right|. \tag{5}$$

If the $m^*(k)$ dependence is known from an experiment, the $E(k)$ dependence can be derived by the numerical integration

$$E(k)=\int_0^k \frac{x}{m^*(x)}dx+E(k=0) \tag{6}$$

where $E(k=0)$ is the energy gap as obtained, e.g., from the absorption experiments. An example of reflectivity data is shown in Fig. 10. We analyze this spectrum using the Drude model for the dielectric function to determine the plasma frequency ω_p. We were able to reproduce the reflectivity

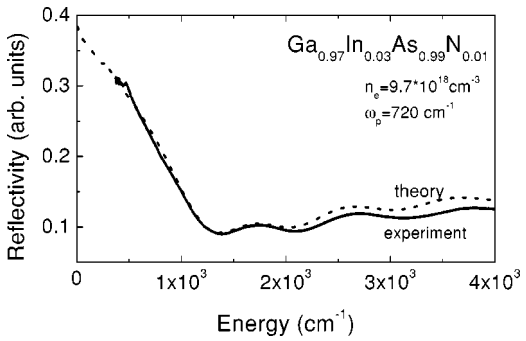

FIG. 10. Reflectivity spectrum in infrared for an $In_{0.03}Ga_{0.97}As_{0.99}N_{0.01}$ sample. Solid line: experimental data. Dotted line: result of fitting.

fringes using the layer thickness measured in scanning tunneling microscopy (SEM) and the high-frequency dielectric constant of GaAs, $\epsilon=10.9$. This indicates that in the energy range of 1000–4000 cm^{-1} the dielectric function is not affected by the small amount of N and In in our samples. The plasma frequency ω_p is determined by the effective mass at the Fermi level and the electron density, n_e.[53] The well-known expression for ω_p yields

$$m_{expt}^*(k_F)=\frac{n_e(k_F)e^2}{\omega_p^2\epsilon_0\epsilon_\infty}, \tag{7}$$

where e is the electron charge, n_e is the electron concentration, ϵ_∞ is the high-frequency dielectric constant, and k_F is the wave vector at the Fermi surface. For an isotropic conduction band k_F is related to the electron n_e concentration through the relation $n_e(k_F)=k_F^3/3\pi^2$. The dependence of the electron effective mass on the Fermi wave vector k_F in $In_{0.03}Ga_{0.97}As_{0.99}N_{0.01}$ samples is shown in Fig. 11. Also, the literature data on the effective mass in GaAs are presented in the same figure. We find a very large, almost fourfold increase of the effective mass in the heavily doped $In_{0.03}Ga_{0.97}As_{0.99}N_{0.01}$ sample with $n_e=2\times10^{19}$ cm^{-3}. This can be compared with a slight increase of the effective mass in GaAs. The small increase can be understood in terms of the $\mathbf{k}\cdot\mathbf{p}$ interaction between the Γ_6 conduction band and Γ_8 valence band. With the experimentally determined $m_{expt}^*(k_F)$

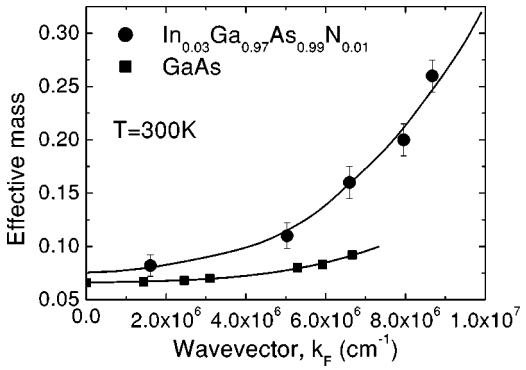

FIG. 11. The effective mass m_{expt}^* vs Fermi wave vector for $In_{0.03}Ga_{0.97}As_{0.99}N_{0.01}$ (dots) (this work) and for GaAs (squares) (after Ref. 46).

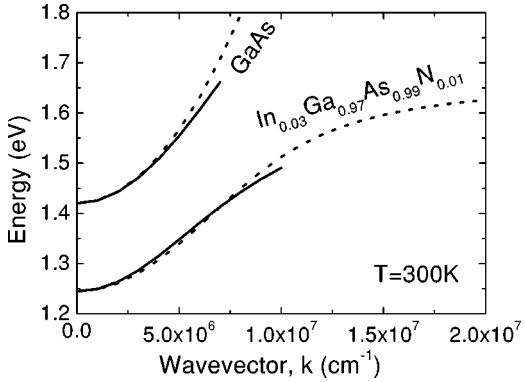

FIG. 12. Experimental DOS calculated from $m^*_{expt}(k)$ solid line (integral). Dotted line for GaAs, parabolic model; dotted line for $In_{0.03}Ga_{0.97}As_{0.99}N_{0.01}$, BAC model.

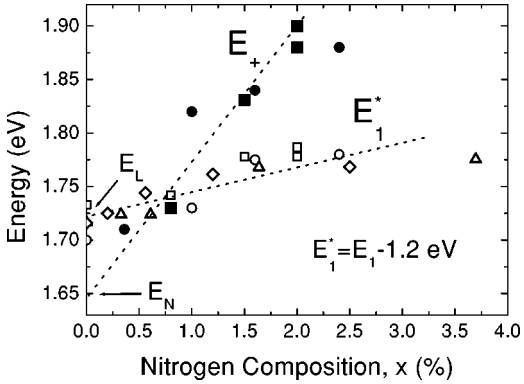

FIG. 13. The energy dependence of the E_+: dots (this work), squares (after Ref. 16), and $E_1^*=E_1-1.2$ eV, circles (this work), open squares (after Ref. 16), open diamonds (after Ref. 17), and open triangles (after Ref. 18).

in $In_{0.03}Ga_{0.97}As_{0.99}N_{0.01}$ and GaAs we use Eq. (6) to calculate the $E(k)$ dependence for the lowest conduction band. The results are shown in Fig. 12. For the absorption edges $E(k=0)$ we have adopted the well-known value of 1.42 eV for GaAs (Ref. 46) and used the measured value of 1.24 eV for undoped $In_{0.03}Ga_{0.97}As_{0.99}N_{0.01}$. The solid lines in Fig. 12 represent the $E(k)$ dispersions deduced from $m^*_{expt}(k_F)$ whereas the dotted lines are the results of calculations. For GaAs a parabolic conduction band with a constant effective mass $m^*=0.065m_0$ has been assumed. The $E(k)$ dependence in $In_{0.03}Ga_{0.97}As_{0.99}N_{0.01}$ was calculated using Eq. (1) and the previously determined parameters $E_N=1.65$ eV and $C_{MN}=2.7$ eV. We find excellent agreement between experimentally determined and theoretically calculated dispersions for the lower conduction subband in $In_{0.03}Ga_{0.97}As_{0.99}N_{0.01}$. The fact that this very good agreement has been achieved with an independently determined set of parameters provides a strong endorsement for the BAC model.

VI. DISCUSSION

We have shown in the preceding sections that all our experimental results are well explained by the BAC model of the electronic structure of $IIIN_xV_{1-x}$ semiconductor alloys. The model is in many respects similar to the ''many-impurity'' Anderson model that has been used to consider the electronic structure of a system of randomly distributed impurities interacting with extended bands.[31,54] The many-impurity model is an extension of the well-known periodic Anderson model[55] that has been widely used to calculate the electronic structure of heavy-fermion metals. In the many-impurity model the randomness in the impurity distribution is typically treated within the CPA. The approximation restores the periodicity of the system and the wave vector as a quantum number, greatly simplifying the theoretical treatment of the electronic structure of such random systems. The price of this simplification is a level broadening resulting from the finite lifetimes of the electronic states. It should be emphasized that in both periodic and many-impurity modes the dispersion relations $E(k)$ are exactly the same as in Eq. (1) derived within the BAC model (see, e.g., Refs. 31 and 56). An important quantitative difference between those two cases is that the C_{MN} in $IIIN_xV_{1-x}$ alloys is about two orders of magnitude larger than a typical hybridization constant in heavy-fermion systems. The main objective of the existing theoretical calculations based on the empirical pseudopotential and/or local density approximation was to reproduce the experimentally observed N-induced band gap reduction in InGaAsN alloys.[21,22,36–38] None of these calculations was able to convincingly identify the energy level responsible for the E_+ absorption edge. As is seen in Fig. 4(b), E_+ transitions correspond to a single, very-well-resolved absorption edge. This edge certainly could not be a ''convolution'' of several different optical transitions as proposed in Ref. 36. To further compare the LDA-based theories with the experiment we use the most recent, large-scale calculations that cover the N composition range relevant to the experiment.[38] The calculations were able to account for the downward shift of the fundamental band edge. Among the calculated higher-energy levels, shown in Fig. 3 of Ref. 38, $a1(2)$ is the only level that has a large enough component of the Γ_6 wave function to be considered a candidate for the final state of the E_+ transitions. However, the calculated energy of this level is constant in the composition range up 1.6%. This is in clear disagreement with the experiment where, as is shown in Fig. 9 the E_+ edge exhibits a large upward shift in the same N composition range. The proximity of the L minimum energy to the E_N level has led to suggestions that the optical transitions to N-perturbed L minimum states are responsible for the E_+ absorption edge. To investigate this in more detail we plot in Fig. 13 the energy $E_1^*=E_1-1.2$ eV which is the E_1 critical point energy measured from the top of the valence band at the Γ point. Although E_1^* is not exactly the energy of the L minimum but rather the energy of the conduction band on a L direction at the E_1 CP, its change with N content should reflect the magnitude of the shift of the L minimum energy as well. The E_+ edge energy as function of the N composition is also shown in this figure. It is clearly seen that E_1^* shows a much weaker N dependence than E_+, suggesting a much different composition dependence for the final states for E_1 and E_+ optical transitions. This result eliminates the possibility that the L minimum could be a final state for E_+ transitions. Among all the theoretical models of the

electronic structure of $III N_x V_{1-x}$, the BAC model provides the most simple analytic method to calculate the conduction band dispersion that can be compared with the experimental data. In fact, so far there has been no attempt within the LDA approach to calculate the $E(k)$ dependence in InGaAsN alloys. It has been argued only that the experimentally observed large increase of the electron effective mass can be qualitatively understood by an admixture of the heavy-mass L and X minimum states to the lowest conduction band minimum at Γ.

VII. SUMMARY AND CONCLUSIONS

Our experimental results show that incorporation of a few percent of N into InGaAs to form InGaAsN alloys leads to a drastic modification of the conduction band density of states close to the Γ band edge. The conduction band is split into two subbands with highly nonparabolic dispersions. In contrast the energies of the higher-lying L and X minima are not significantly affected by these small amounts of nitrogen. The variation of the energies of L and X minima with N content can be well understood within the virtual crystal approximation for InGaAsN alloys. The results also show that incorporation of N does not have any significant effect on the valence band structure as exemplified by a constant N-independent value of the spin-orbit splitting. An analysis of the experimental data showed that the N-induced effects can be well accounted for by the BAC model describing the conduction band structure in terms of hybridization between highly localized A_1 states of N and the extended states of the host semiconductor matrix. Using the previously determined hybridization parameter C_{MN} the BAC model could account for the composition and temperature dependence of the optical transitions. It also provided an accurate description of the experimentally determined dispersion $E_-(k)$ for the lower conduction subband.

ACKNOWLEDGMENTS

This work was supported by the Polish KBN Grant No. 5 P03B 057 20, the Austrian Bundesministerium für Bildung, Wissenschaft und Kultur, Vienna, and its ÖAD branch, and the Gesellschaft fur Mikroelektronik, Vienna. The work at Berkeley Lab was supported by ''Photovoltaic Materials Focus Area'' in the DOE Center of Excellence for the Synthesis and Processing of Advanced Materials, Office of Science, Office of Basic Energy Sciences, Division of Materials Sciences of the U.S. Department of Energy under Contract No. DE-AC03-76SF00098.

[1] M. Weyers, M. Sato, and H. Ando, Jpn. J. Appl. Phys., Part 2 **31**, L853 (1992).
[2] Su-Huai Wei and A. Zunger, Phys. Rev. Lett. **76**, 664 (1996).
[3] M. Kondow, K. Uomi, K. Hosomi, and T. Mozume, Jpn. J. Appl. Phys., Part 2 **33**, L1056 (1994).
[4] I.A. Buyanova, W.M. Chen, and B. Monemar, MRS Internet J. Nitride Semicond. Res. **6**, 2 (2001).
[5] N. Baillargeon, K.Y. Cheng, G.F. Hofler, P.J. Pearah, and K.C. Hsieh, Appl. Phys. Lett. **60**, 2540 (1992).
[6] W.G. Bi and C.W. Tu, Appl. Phys. Lett. **69**, 3710 (1996).
[7] W.G. Bi and C.W. Tu, J. Appl. Phys. **80**, 1934 (1996).
[8] K.M. Yu, W. Walukiewicz, J. Wu, J.W. Beeman, J.W. Ager, E.E. Haller, W. Shan, H.P. Xin, and C.W. Tu, Appl. Phys. Lett. **78**, 1077 (2001).
[9] J.C. Harmand, G. Ungaro, J. Ramos, E.V.K. Rao, G. Saint-Girons, R. Teissier, G. Le Roux, L. Largeau, and G. Patriarche, J. Cryst. Growth (to be published).
[10] B.N. Murdin, M. Karmal-Saadi, A. Lindsay, E.P. O'Reilly, A.R. Adams, G.J. Nott, J.G. Crowder, C.R. Pidgeon, I.V. Bradley, J-P.R. Wells, T. Burke, A.D. Johnson, and T. Ashley, Appl. Phys. Lett. **78**, 1568 (2001).
[11] Steven R. Kurtz, A.A. Allerman, E.D. Jones, J.M. Gee, J.J. Banas, and B.E. Hammons, Appl. Phys. Lett. **74**, 729 (1999).
[12] A. Wagner, C. Ellmers, F. Hohnsdorf, J. Koch, C. Agert, S. Leu, M. Hofmann, W. Stolz, and W.W. Ruhle, Appl. Phys. Lett. **76**, 271 (2000).
[13] J.F. Geisz, D.J. Friedman, J.M. Olson, S.R. Kurtz, and B.M. Keyes, J. Cryst. Growth **195**, 401 (1998).
[14] H. Gruning, L. Chen, Th. Hartman, P.J. Klar, W. Heimbrodt, F. Hohnsdorf, J. Koch, and W. Stolz, Phys. Status Solidi B **215**, 39 (1999).
[15] J. Perkins *et al.* (unpublished).
[16] W. Shan, W. Walukiewicz, K.M. Yu, J.W. Ager III, E.E. Haller, J.F. Geisz, D.J. Friedman, J.M. Olson, Sarah R. Kurtz, and C. Nauka, Phys. Rev. B **62**, 4211 (2000).
[17] W.K. Hung, M.Y. Chern, Y.F. Chen, Z.L. Yang, and Y.S. Huang, Phys. Rev. B **62**, 13 028 (2000).
[18] G. Leibiger, V. Gottschalch, B. Rheinlander, J. Sik, and M. Schubert, Appl. Phys. Lett. **77**, 1650 (2000).
[19] S Sakai, Y. Ueta, and Y Terauchi, Jpn. J. Appl. Phys., Part 1 **32**, 4413 (1993).
[20] J.A. Van Vechten and T.K Bergstresser, Phys. Rev. B **8**, 3351 (1970).
[21] A. Rubio and M.L. Cohen, Phys. Rev. B **51**, 4343 (1995).
[22] J. Neugebauer and C.G. Van de Walle, Phys. Rev. B **51**, 10 568 (1995).
[23] L. Bellaiche, S.-H. Wei, and A. Zunger, Phys. Rev. B **54**, 17 568 (1996).
[24] P. Perlin, S.G. Subramanya, D.E. Mars, J. Kruger, N.A. Shapiro, H. Siegle, and E.R. Weber, Appl. Phys. Lett. **73**, 3703 (1998).
[25] W. Shan, W. Walukiewicz, J.W. Ager III, E.E. Haller, J.F. Geisz, D.J. Friedman, J.M. Olson, and S.R. Kurz, Phys. Rev. Lett. **82**, 1221 (1999).
[26] E.D. Jones, N.A. Modine, A.A. Allerman, S.R. Kurtz, A.F. Wright, S.T. Tozer, and X. Wei, Phys. Rev. B **60**, 4430 (1999).
[27] J.D. Perkins, A. Mascarenhas, Y. Zhang, J.F. Geisz, D.J. Friedman, J.M. Olson, and S.R. Kurtz, Phys. Rev. Lett. **82**, 3312 (1999).
[28] W. Walukiewicz, W. Shan, J.W. Ager III, D.R. Chamberlin, E.E. Hailer, J.F. Geisz, D.J. Friedman, J.M. Olson, and S.R. Kurtz (unpublished).

[29] W. Shan, W. Walukiewicz, K.M. Yu, J.W. Ager III, E.E. Haller, J.F. Geisz, D.J. Friedman, J.M. Olson, S.R. Kurtz, H.P. Xin, and C.W. Tu, Phys. Status Solidi B **223**, 75 (2001).
[30] E.P. O'Reilly and A. Lindsay, Phys. Status Solidi B **216**, 131 (1999).
[31] M.A. Ivanov and Yu.G. Pogorelov, Zh. Éksp. Teor. Fiz. **7**6, 1010 (1979) [Sov. Phys. JETP **49**, 510 (1979)].
[32] C. Skierbiszewski, P. Perlin, P. Wisniewski, W. Knap, T. Suski, W. Walukiewicz, W. Shan, J.W. Ager, E.E. Haller, J.F. Geisz, D.J. Friedman, J.M. Olson, and S.R. Kurtz, Appl. Phys. Lett. **76**, 2409 (2000).
[33] K.M. Yu, W. Walukiewicz, W. Shan, J.W. Ager III, J. Wu, E.E. Haller, J.F. Geisz, D.J. Friedman, and J.M. Olson, Phys. Rev. B **61**, R13 337 (2000).
[34] W. Shan, W. Walukiewicz, K.M. Yu, J. Wu, J.W. Ager III, E.E. Haller, H.P. Xin, and C.W. Tu, Appl. Phys. Lett. **76**, 3251 (2000).
[35] W. Walukiewicz, W. Shan, K.M. Yu, J.W. Auger III, E.E. Haller, I. Miotkowski, M.J. Seong, H. Alawadhi, and A.K. Ramdas, Phys. Rev. Lett. **85**, 1552 (2000).
[36] T. Mattila, Su-Huai Wei, and Alex Zunger, Phys. Rev. B **60**, R11 245 (1999).
[37] L. Bellaiche, N.A. Modine, and E.D. Jones, Phys. Rev. B **62**, 15 311 (2000).
[38] Lin-Wang Wang, Appl. Phys. Lett. **78**, 1565 (2001).
[39] G. Szwacki and P. Boguslawski (unpublished).
[40] A. Al-Yacoub and L. Bellaiche, Phys. Rev. B **62**, 10 847 (2000).
[41] Y. Zhang, A. Mascarenhas, H.P. Xin, and C.W. Tu, Phys. Rev. B **63**, 161303 (2001).
[42] P. Perlin, P. Wisniewski, C. Skierbiszewski, T. Suski, E. Kaminska, S.G. Subramanya, E.R. Weber, D.E. Mars, and W. Walukiewicz, Appl. Phys. Lett. **76**, 1279 (2000).
[43] Sarah Kurtz, J.F. Geisz, D.J. Friedman, J.M. Olson, A. Duda, N.H. Karam, R.R. King, J.H. Ermer, and D.E. Joslin (unpublished).
[44] I. Suemune, K. Uesugi, W. Walukiewicz, Appl. Phys. Lett. **77**, 3021 (2000).
[45] L. Viña, S. Logothetidis, and M. Cardona, Phys. Rev. B **30**, 1979 (1984).
[46] J.S. Blackmore, J. Appl. Phys. **53**, R123 (1982).
[47] T. Takagi, Jpn. J. Appl. Phys., Part 2 . **17**, 1813 (1978).
[48] D.E. Aspnes and A.A. Studna, Phys. Rev. B **27**, 985 (1983).
[49] L. Viña, C. Umbach, M. Cardona, and L. Vodopyanov, Phys. Rev. B **29**, 6752 (1984).
[50] H. Lee, M.V. Klein, D.E. Aspnes, C.P. Kuq, M. Peanasky, and M.G. Craford, J. Appl. Phys. **73**, 400 (1993).
[51] P. Lautenschlager, M. Garriga, S. Logothetidis, and M. Cardona, Phys. Rev. B **35**, 9174 (1987).
[52] A. Rubio, J.L. Corkill, M.L. Cohen, E.L. Shirley, and S.G. Louie, Phys. Rev. B **48**, 11 810 (1993).
[53] W.G. Spitzer and H.Y. Fan, Phys. Rev. **106**, 882 (1957).
[54] E.V. Kuzmin, S.G. Ovchinnikov, and I.S. Sandalov, Sov. Phys. JETP **46**, 822 (1977).
[55] P.W. Anderson, Phys. Rev. **124**, 41 (1961).
[56] P.S. Riseborugh, Adv. Phys. **49**, 257 (2000).